

# Suzaku Observation of the Diffuse X-Ray Emission from the Open Cluster Westerlund 2: a Hypernova Remnant?

Yutaka FUJITA<sup>1</sup>, Kiyoshi HAYASHIDA<sup>1</sup>, Hiroaki TAKAHASHI<sup>1</sup>, and Fumio TAKAHARA<sup>1</sup>,

<sup>1</sup>*Department of Earth and Space Science, Graduate School of Science,*

*Osaka University, Toyonaka, Osaka 560-0043*

*fujita@vega.ess.sci.osaka-u.ac.jp*

(Received 2009 December 31; accepted 2009 January 1)

## Abstract

We present the analysis of Suzaku observations of the young open cluster Westerlund 2, which is filled with diffuse X-ray emission. We found that the emission consists of three thermal components or two thermal and one non-thermal components. The upper limit of the energy flux of the non-thermal component is smaller than that in the TeV band observed with H.E.S.S. This may indicate that active particle acceleration has stopped in this cluster, and that the accelerated electrons have already cooled. The gamma-ray emission observed with H.E.S.S. is likely to come from high-energy protons, which hardly cool in contrast with electrons. Metal abundances of the diffuse X-ray gas may indicate the explosion of a massive star in the past.

**Key words:** stars: winds, outflows — ISM: cosmic rays — ISM: individual (RCW 49) — ISM: supernova remnants — Galaxy: open clusters and associations: individual (Westerlund 2)

## 1. Introduction

Cosmic-ray particles with energies of  $\lesssim 10^{15}$  eV are thought to be accelerated in our Milky Way. Supernova remnants (SNRs) have long been considered to be the main sources of the galactic cosmic-rays. In fact, their synchrotron emission reveals the existence of high-energy electrons in SNRs (Koyama et al. 1995), and their gamma-ray emission may indicate that of high-energy protons (Aharonian et al. 2004). However, it is not clear to what extent the isolated SNRs could account for the cosmic-ray particles in our Milky Way.

Young open clusters are one of other candidates of the cosmic-ray sources. The HEGRA stereoscopic system of air Čerenkov telescopes has detected a gamma-ray signal inside the core of the OB association Cygnus OB2 (Aharonian et al. 2002). The Milagro gamma-ray

observatory found gamma-ray emission around the young open cluster Berkeley 87 (Abdo et al. 2007). These observations suggest that particles are accelerated around open clusters.

Several models have been proposed as the origin of the gamma-ray emission from young open clusters. The gamma-rays could be produced through collisions of protons accelerated at shocks in massive stellar winds in the cluster (Giovannelli et al. 1996). Some of the protons may penetrate the winds of the massive stars toward the stellar surfaces and produce gamma-rays through hadronic interactions in the dense parts of the winds (Torres et al. 2004). High-energy leptons may contribute to the gamma-ray emission through inverse Compton scattering (Bednarek 2007; Manolakou et al. 2007). In addition to the stellar winds, pulsars in a cluster might be responsible for the gamma-ray emission (Bednarek 2003). The gamma-rays could also be produced through the photodisintegration of highly boosted nuclei followed by daughter deexcitation (Anchordoqui et al. 2007).

Westerlund 2 is one of the clusters from which gamma-ray emission has been detected with H.E.S.S. (Aharonian et al. 2007). It is ionizing the large H II region RCW 49 (NGC 3247). The gamma-ray emission is extended ( $\sim 0.2^\circ$ ), and the whole cluster is buried in it. Observations in the X-ray band are crucial to find the origin of the diffuse gamma-ray emission from the cluster and the mechanism of particle acceleration. In particular, the strength of non-thermal X-ray emission can be used to discriminate between the hadronic and the leptonic origin of the gamma-rays (Bednarek 2007), and estimate the time-scale of particle acceleration (Manolakou et al. 2007). In the X-ray band, although the cluster has been observed with Einstein (Hertz & Grindlay 1984; Goldwurm et al. 1987) and ROSAT (Belloni & Mereghetti 1994), strict constraint on non-thermal emission has not been obtained. With Chandra, Townsley et al. (2005) studied diffuse X-ray emission  $\lesssim 5'$  from the center of Westerlund 2 and found that the spectrum could be represented by both thermal and non-thermal emission.

In this paper, we report the results from Suzaku observations of Westerlund 2. Since Suzaku has a large collecting area and low background (Mitsuda et al. 2007), it is the best instrument for observations of dim and diffuse X-ray emission. This paper is organized as follows. The observation is presented in section 2. In section 3, we explain the details of the spectral analysis. Section 4 is devoted to discussion. Conclusions are summarized in section 5. We assume that the distance to the cluster is 5.4 kpc unless otherwise mentioned (Furukawa et al. 2009), although there is a debate about it ( $\sim 2\text{--}8$  kpc; Piatti et al. 1998; Dame 2007; Tsujimoto et al. 2007; Rauw et al. 2007; Ascenso et al. 2007). At a distance of 5.4 kpc,  $1'$  corresponds to 1.6 pc.

## 2. Observations

Westerlund 2 was observed with Suzaku on 2008 August 9–11 and 2009 February 4–5. The exposure times for the two observations are 73.7 ks and 33.5 ks, respectively. The data of the two observations are dealt together in the following analysis. Suzaku has three working

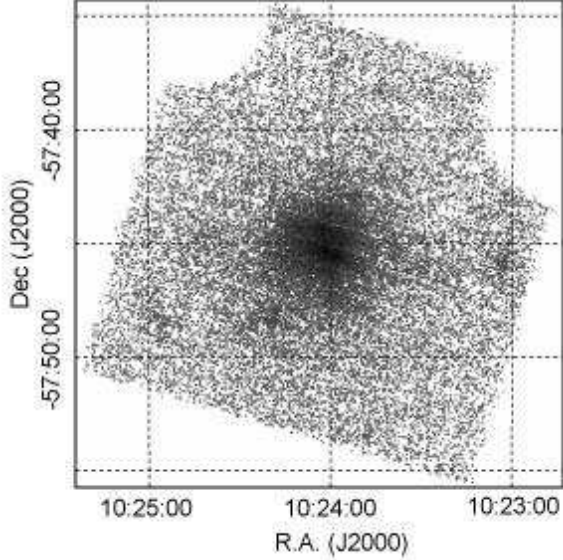


**Fig. 1.** XIS 0 raw image of Westerlund 2. The image is not corrected for vignetting and background. The calibration sources at the corner of the field were excluded.

XIS CCDs (Koyama et al. 2007). Two of them (XIS 0, and 3) are front-illuminated (FI) and one (XIS 1) is back-illuminated (BI). The XIS was operated in the normal full-frame clocking mode. The edit mode was  $3 \times 3$  and  $5 \times 5$  and we combined the data of both modes for our analysis. We employed the following calibration files: XIS (20090203) and XRT (20080709). Events with ASCA grades of 0, 2, 3, 4, and 6 were retained. We excluded the data obtained at the South Atlantic Anomaly, during Earth occultation, and at the low elevation angles from Earth rim of  $< 5^\circ$ . We further excluded the data with elevation angle from the rim of the shining Earth smaller than  $20^\circ$ . Figure. 1 is a raw XIS image of Westerlund 2.

### 3. Spectral Analysis

We analyze the spectrum of the diffuse emission around Westerlund 2. Since the angular resolution of the XIS is moderate ( $\sim 2'$ ), we need to estimate the amount of X-ray emission from point sources that contaminate the diffuse X-ray emission from the cluster (e.g. Hamaguchi et al. 2007; Hyodo et al. 2008; Ezoe et al. 2009). Moreover, since the diffuse emission is faint, the background spectrum must be constructed carefully. Errors on fitted spectral parameters are given at the 90% confidence level from now on.

#### 3.1. Contamination from Point Sources

In order to estimate the contamination of the point sources, we used Chandra archive data of Westerlund 2 (ID 3501, 6410, and 6411). In order to extract the positions and spectra

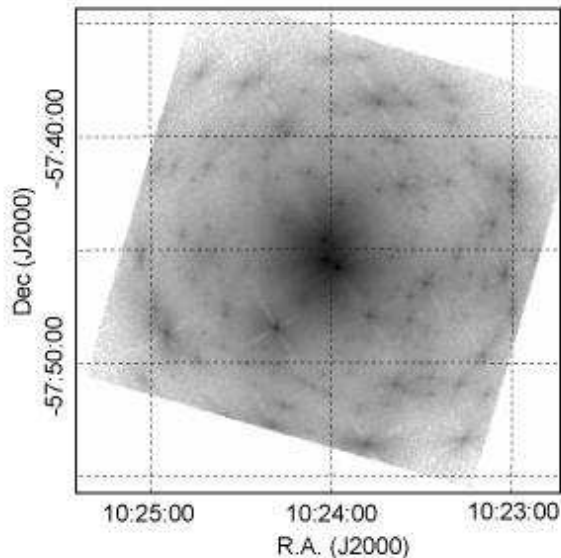


**Fig. 2.** Simulated XIS 0 image of Westerlund 2. Only photons from point sources are included. The exposure time is assumed to be 22 Ms in order to emphasize the X-ray structure.

of the point sources, we used the ACIS Extract (AE) software package<sup>1</sup> (Broos et al. 2002). The procedures used in AE are described in Townsley et al. (2003) and Getman et al. (2005). AE detected 930 point sources from the data of the three observations ( $\gtrsim 10^{-15}$  ergs $^{-1}$  cm $^{-2}$  in the 2–10 keV band). AE produces spectral files for individual point sources. For the 9 brightest sources with photon counts of  $> 300$ , we can treat their spectra separately. For fainter point sources, it is difficult to obtain their individual spectra because of their small photon counts. Thus, we combined their spectral files by MATHPHA included in FTOOLS. For that purpose, we used the data of 570 point sources, which are well-separated from their neighboring sources, and their background spectra can be obtained around them. We assume that the spectral shapes of the individual fainter sources are the same as that of the combined spectrum but their luminosities are different.

Using the positional and spectral data, we simulate an XIS observation of the point sources with the XIS simulator MKPHLIST and XISSIM (Ishisaki et al. 2007). The produced event files include both positional and energy information of photons only from the point sources. Figure 2 is the simulated XIS image of Westerlund 2 that includes only photons from the point sources.

---

<sup>1</sup> The ACIS Extract software package and User’s Guide are available online at [http://www.astro.psu.edu/xray/docs/TARA/ae\\_users\\_guide.html](http://www.astro.psu.edu/xray/docs/TARA/ae_users_guide.html).

### 3.2. Background Spectrum

Since the TeV gamma-ray emission from Westerlund 2 covers the entire XIS field (Aharonian et al. 2007), we used the spectrum of a blank region around SWIFTJ1010.1–5747 obtained with Suzaku ( $10^{\text{h}}10^{\text{m}}55^{\text{s}}.4$ ,  $-57^{\circ}51^{\text{m}}14^{\text{s}}$  [J2000.0]) as the background of Westerlund 2. The exposure time is 38 ks. We call this region the blank region. This region is  $\sim 1.7^{\circ}$  away from Westerlund 2 ( $10^{\text{h}}23^{\text{m}}59^{\text{s}}.0$ ,  $-57^{\text{d}}44^{\text{m}}40^{\text{s}}$ ). The Galactic coordinates of Westerlund 2 and the blank region are  $(l, b) = (284.25^{\circ}, -0.32^{\circ})$  and  $(282.87^{\circ}, -1.38^{\circ})$ , respectively. Westerlund 2 and the blank region are both affected by the Galactic Ridge X-ray Emission (GRXE; Revnivtsev et al. 2006).

We subtract the non-X-ray instrumental background (NXB) from the spectrum of the blank region. The NXB is constructed from night Earth data, and is generated by the routine `XISNXBGEN` included `FTOOLS`, considering the time-variation of the NXB (Tawa et al. 2008). We calculate the effective area for the Suzaku XIS chips using `XISSIMARFGEN`, which provides the ancillary response file (ARF) through Monte Carlo simulations (Ishisaki et al. 2007). After the NXB is subtracted and removing a few noticeable point sources brighter than  $\sim 10^{-13} \text{ ergs s}^{-1} \text{ cm}^{-2}$  in the 2–10 keV band, we fit the X-ray emission from the blank region with spectral components of the GRXE, the cosmic X-ray background (CXB), and the local hot bubble (LHB). We assume that the contribution of faint point sources ( $\gtrsim 3 \times 10^{-15} \text{ ergs s}^{-1} \text{ cm}^{-2}$  in the 2–10 keV band), which Chandra could have detected with an exposure time of  $\sim 100$  ks, to the Suzaku spectrum of the blank region can be ignored, because Ebisawa et al. (2005) found that the contribution of point sources brighter than  $\sim 3 \times 10^{-15} \text{ ergs s}^{-1} \text{ cm}^{-2}$  (2–10 keV) to the GRXE is only  $\sim 10\%$  (see also Revnivtsev et al. 2009). The spectrum of the GRXE can be represented by two thermal models (VAPEC), and two absorptions (PHABS) with a combination of `PHABS * VAPEC + PHABS * VAPEC`. The spectra of the CXB and the LHB are represented by an absorbed power-law model (`PHABS * POWER`) and a thermal model (APEC), respectively. For the CXB spectrum, we use the results of Kushino et al. (2002) for `POWER` and those of Dickey & Lockman (1990) and Kalberla et al. (2005) for `PHABS`. Since the region around Westerlund 2 is affected by the GRXE, we use the average of the LHB spectra at positions  $\pm 5^{\circ}$  away from Westerlund 2 in the direction of galactic latitude (Snowden et al. 1998). The temperature of the LHB is 0.1 keV. The parameters for the GRXE in the blank region are shown in Table 1. The best-fit values for the GRXE are derived by fixing all the parameters of the spectra of the CXB and the LHB at their best-fit values. For the groupings of metals, we refer to the results in Ebisawa et al. (2005). For the errors, we include not only statistical errors but also systematic errors made by a spatial variation of the intensity of the CXB. Kushino et al. (2002) estimated the spatial variation of the CXB is 6.49% for the ASCA field. We adjusted the value to be consistent with the XIS field. Moreover, since we masked the regions around bright point sources ( $\sim 20\%$  of the XIS field), we consider the decrease of the effective area in the field. Thus, we adopt the systematic error of 16% for the CXB flux.

**Table 1.** Best-fit parameters for the GRXE

Component	Parameter	
Soft	$kT$ (keV)	$0.41^{+0.28}_{-0.04}$
	Abundance except for Ne, Mg, Si (solar)	0.044*
	Ne (solar)	$0.22^{+0.07}_{-0.06}$
	Mg (solar)	$0.11^{+0.09}_{-0.08}$
	Si (solar)	$0.25^{+0.35}_{-0.25}$
	$N_H$ ( $10^{22}$ cm $^{-2}$ )	$0.16^{+0.13}_{-0.16}$
	Observed flux $^\dagger$ ( $10^{-8}$ ergs cm $^{-2}$ s $^{-1}$ sr $^{-1}$ )	$1.7^{+0.1}_{-0.0}$
Intrinsic flux $^\dagger$ ( $10^{-8}$ ergs cm $^{-2}$ s $^{-1}$ sr $^{-1}$ )	$2.8^{+0.1}_{-0.2}$	
Hard	$kT$ (keV)	$8.9^{+4.3}_{-2.4}$
	Abundance except for Fe (solar)	0.17*
	Fe (solar)	$1.5^{+1.1}_{-0.6}$
	$N_H$ ( $10^{22}$ cm $^{-2}$ )	$0.76^{+0.48}_{-0.41}$
	Observed flux $^\dagger$ ( $10^{-8}$ ergs cm $^{-2}$ s $^{-1}$ sr $^{-1}$ )	$6.3^{+0.9}_{-0.7}$
	Intrinsic flux $^\dagger$ ( $10^{-8}$ ergs cm $^{-2}$ s $^{-1}$ sr $^{-1}$ )	$8.0^{+1.2}_{-1.2}$
	$\chi^2/\text{d.o.f.}$	353/331

\* Fixed at the values of the GRXE in Table 8 of Ebisawa et al. (2005).

$^\dagger$  In the 0.7–10 keV band.

Considering the distance between Westerlund 2 and the blank region on the sky, we need to take account of spatial variation of the GRXE, when we use the spectrum of the blank region as the background spectrum of Westerlund 2. In the 3–20 keV band, the flux of the GRXE in the blank region is  $2.0 \pm 0.3 \times 10^{-11}$  ergs cm $^{-2}$  s $^{-1}$  deg $^{-2}$  and is consistent with the value obtained with RXTE ( $2.3 \pm 0.4 \times 10^{-11}$  ergs cm $^{-2}$  s $^{-1}$  deg $^{-2}$ ; Revnivtsev et al. 2006). At the position of Westerlund 2, the X-ray flux of the GRXE is  $1.8 \pm 0.4 \times 10^{-11}$  ergs cm $^{-2}$  s $^{-1}$  deg $^{-2}$  (Revnivtsev et al. 2006), which is  $\sim 60\%$  of that of the CXB. Thus, we change the normalization of the GRXE spectrum of the blank region accordingly, considering the systematic error of the flux. Moreover, we include the systematic error of the CXB flux. Since the area of the masked regions in the Westerlund 2 field is different from that in the blank region (see the next subsection), we adopt an error of 18%.

### 3.3. Diffuse Emission from Westerlund 2

Including the leaked X-rays from the point sources and the X-ray background emission (GRXE, CXB, and LHB) estimated above, we analyze the XIS spectrum of the diffuse emission from Westerlund 2. We refer to the diffuse X-ray emission around Westerlund 2 excluding those unwanted components as the gas component. We calculate the effective area of the Suzaku XIS chips using XISSIMARFGEN. All spectra were rebinned to give a minimum of 20 raw counts per

spectral bin to allow  $\chi^2$  statistics to be applied. The NXB spectrum calculated with `XISNXBGEN` is subtracted from the spectrum. In order to minimize the contamination from the point sources, we mask the central region of the cluster ( $< 2'$  from the center). We also mask 88 bright point sources with circles of  $0.5' - 2'$ . In total, we mask  $\sim 40\%$  of the XIS field.

In the spectral fits, FI and BI XIS spectra were respectively summed. We fix the parameters for the leaked stellar emission and the X-ray background except for the normalizations of the GRXE and the CXB spectra, which we allow to vary according to the systematic errors estimated in section 3.2. We find that the spectrum of the gas component can be represented by three thermal models or two thermal models and one power-law model with absorptions. That is,  $\text{PHABS} * \text{VAPEC} + \text{PHABS} * (\text{VAPEC} + \text{VAPEC})$  or  $\text{PHABS} * \text{VAPEC} + \text{PHABS} * (\text{VAPEC} + \text{POWER})$ . We call the former 3T model and the latter 2TP model. In each model, metal abundances are the same among thermal models with different temperatures. The abundances of N and O are linked to that of C, and the abundance of Ni is linked to that of Fe. The abundances of He, Al, Ar, and Ca are fixed at the solar values. The parameters of these models are common between the two types of XISs (FI and BI), except for the normalization of the highest temperature VAPEC model (3T) or the power-law model (2TP), which is the main component of the spectra.

The results of the fits are shown in Figure 3 and Table 2. The temperatures of the thermal components for 3T model are  $kT_1$ ,  $kT_2$ , and  $kT_3$ . Their intrinsic fluxes in the 0.7–10 keV band are  $f_1$ ,  $f_2$ , and  $f_3$ , respectively. We assume that the X-ray emission comes from the entire XIS field ( $17'.8 \times 17'.8$ ), and we make up the X-rays from the masked regions with those from the surrounding regions. For 2TP model,  $kT_3$  and  $f_3$  are replaced by the photon index ( $\Gamma$ ) and the non-thermal flux ( $f_{\text{NT}}$ ), respectively. The absorption  $N_{H1}$  is the one for the lower temperature component ( $kT_1$ ), and  $N_{H2}$  is the one for the higher. The errors in Table 2 include both the statistical errors and the systematic errors from the uncertainties about the GRXE and the CXB (section 3.2). The low metal abundances compared with the solar values are similar to those of the Carina Nebula, which also contains massive stars (Hamaguchi et al. 2007). It is to be noted that the contributing ratio of flux of the gas component, the leaked stellar emission, and the X-ray background to the total spectrum excluding the NXB in the 2–10 keV band is 43:14:43 (see Figure 4).

Nazé et al. (2008) monitored bright stars in Westerlund 2 and found that X-ray luminosities of several of the brightest stars vary about 30%. However, the sum of the luminosities of the 9 brightest stars in Westerlund 2 is only  $\sim 30\%$  of the total stellar luminosity of Westerlund 2. Moreover, it is unlikely that the flux variation of the stars synchronizes. Considering the fact that only 14% of the diffuse X-ray emission around Westerlund 2 is attributed to the leaked stellar emission, we can ignore the flux variation of the stars in the spectral analysis.

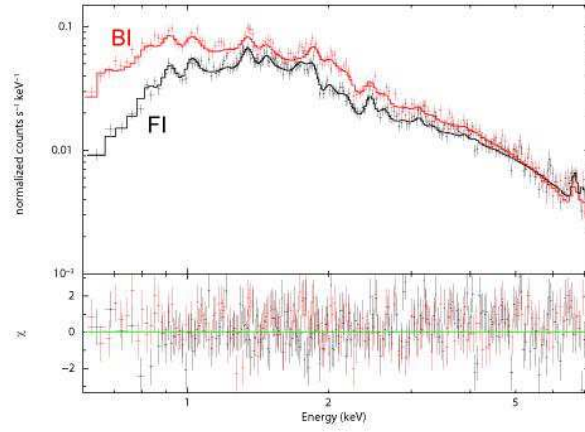


**Fig. 3.** X-ray spectrum of the diffuse emission from Westerlund 2 (crosses). The NXB spectrum is subtracted. The result of the fit is shown by the lines, while the lower panel plots the residuals divided by the  $1\sigma$  errors.

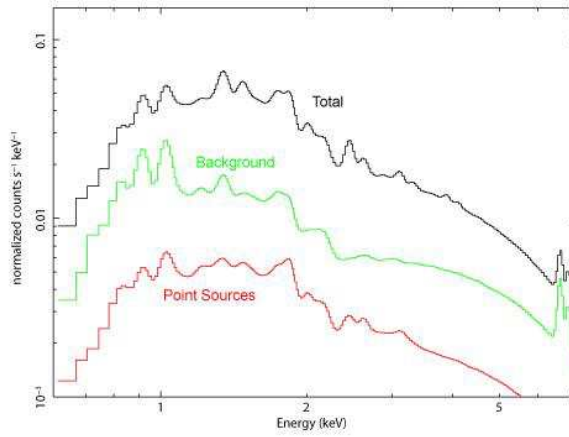


**Fig. 4.** Contributions of the point sources (red) and the X-ray background (green) to the FI spectrum shown in Fig. 3 (black).

**Table 2.** Best-fit parameters for the gas component

Parameter	3T	2TP
$N_{H1}$ ( $10^{22}$ cm $^{-2}$ )	$0.96^{+0.16}_{-0.37}$	$1.1^{+0.0}_{-0.5}$
$kT_1$ (keV)	$0.12^{0.04}_{-0.01}$	$0.12^{+0.04}_{-0.01}$
$N_{H2}$ ( $10^{22}$ cm $^{-2}$ )	$1.1^{+0.4}_{-0.3}$	$1.4^{+0.2}_{-0.4}$
$kT_2$ (keV)	$0.88^{+0.21}_{-0.15}$	$1.0^{+0.3}_{-0.1}$
$kT_3$ (keV)	$4.2^{+2.1}_{-1.2}$	.....
$\Gamma$	.....	$2.2^{+0.4}_{-0.4}$
C, N, O (solar)	$0.24^{+0.71}_{-0.20}$	$0.57^{+1.2}_{-0.43}$
Ne (solar)	$0.04^{+0.09}_{-0.04}$	$0.07^{+0.17}_{-0.07}$
Mg (solar)	$0.46^{+0.32}_{-0.17}$	$0.77^{+0.98}_{-0.42}$
Si (solar)	$0.35^{+0.20}_{-0.12}$	$0.38^{+0.47}_{-0.19}$
S (solar)	$0.86^{+0.43}_{-0.32}$	$0.78^{+1.2}_{-0.31}$
Fe, Ni (solar)	$0.0^{+0.13}_{-0.0}$	$0.0^{+0.33}_{-0.0}$
$f_1$ (ergs cm $^{-2}$ s $^{-1}$ )	$8.7^{+0.0}_{-1.7} \times 10^{-12}$	$1.3^{+0.3}_{-0.4} \times 10^{-11}$
$f_2$ (ergs cm $^{-2}$ s $^{-1}$ )	$2.2^{+0.4}_{-0.0} \times 10^{-12}$	$3.0^{+0.3}_{-0.2} \times 10^{-12}$
$f_3$ (ergs cm $^{-2}$ s $^{-1}$ )	$4.6^{+0.5}_{-0.8} \times 10^{-12}$	.....
$f_{NT}$ (ergs cm $^{-2}$ s $^{-1}$ )	.....	$5.4^{+0.7}_{-1.4} \times 10^{-12}$
$\chi^2/\text{d.o.f.}$	1719.56/1725	1729.06/1725

## 4. Discussion

### 4.1. Upper limit of Non-thermal Flux

We found that the spectrum of the gas component of Westerlund 2 can be represented by three thermal models (3T) or two thermal models and one power-law model (2TP). Since the power-law component in 2TP model can be replaced by a thermal component, the power-law component when the contributions of the GRXE and the CXB to the total spectrum are minimum gives the upper limit of non-thermal X-ray flux from the cluster. Assuming that the non-thermal emission comes from the entire XIS field, the upper limit of the flux is  $f_{NT} < 2.6 \times 10^{-12}$  ergs cm $^{-2}$  s $^{-1}$  (0.7–2 keV) and  $6.1 \times 10^{-12}$  ergs cm $^{-2}$  s $^{-1}$  (0.7–10 keV). In this estimation, we compensate for the X-rays from the masked regions with those from the surrounding regions.

Although the photon counts are small for detailed spectral analysis, we found that X-ray surface brightness of a region that is  $> 8'$  away from the cluster in the XIS field (the center of the circle is shifted from the cluster center according to the surface brightness contours) is comparable to the one estimated from the blank region. Thus, the emission from the outside of the XIS field does not much contribute to the total diffuse emission from Westerlund 2.

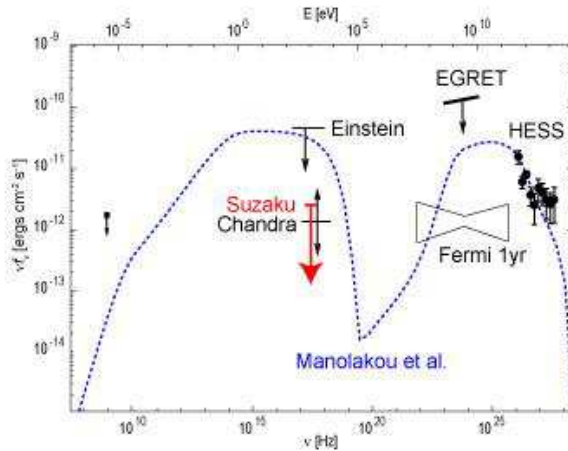


**Fig. 5.** Multi-wavelength measurements of Westerlund 2 (radio: Whiteoak & Uchida 1997; Einstein: Goldwurm et al. 1987; Chandra: Townsley et al. 2005; Suzaku: this study [0.7–2 keV]; EGRET; Hartman et al. 1999; H.E.S.S.: Aharonian et al. 2007). Fermi one year flux sensitivity is shown by the thin solid line<sup>3</sup>. A theoretical prediction of Manolakou et al. (2007) is shown by the dotted line (their model of  $t = 10^5$  yr).

We also analyzed the HXD data of Suzaku. Adopting a systematic uncertainty of 5% for the NXB, we found that the upper limit of the X-ray flux from Westerlund 2 in the 15–40 keV band is  $5 \times 10^{-12}$  ergs cm<sup>-2</sup> s<sup>-1</sup>, excluding the CXB and the GRXE. We assumed that the spectrum of the CXB is represented by a power-law model multiplied by a HIGHECUT model in XSPEC. We adopted the power-law index of 1.29, the power-law normalization of  $9.412 \times 10^{-3}$  photons cm<sup>-2</sup> s<sup>-1</sup> FOV<sup>-1</sup>keV<sup>-1</sup>, and the e-folding energy of 40 keV, following a standard model<sup>2</sup>. The spectrum of the GRXE is extrapolated from the one in the soft X-ray band. The upper limit of the flux from Westerlund 2 can be compared with the extrapolated values of 3T and 2TP models ( $\lesssim 4 \times 10^{-12}$  ergs cm<sup>-2</sup> s<sup>-1</sup>). Considering that the HXD has a wider field ( $34' \times 34'$ ) than the XIS, this result indicates that it is unlikely that strong hard X-ray emission extends beyond the XIS field.

#### 4.2. Comparison with Previous Observations

In Figure 5, we present multi-wavelength measurements of Westerlund 2. The radio flux is considered as an upper limit, because it could only partially include the non-thermal radio flux produced by the energetic electrons (Whiteoak & Uchida 1997). The Einstein observations probably overestimate the diffuse flux, because the limited spatial resolution may not allow the subtraction of the point sources well enough (Goldwurm et al. 1987). The flux obtained with EGRET may also need to be regarded as an upper limit, because of its low spatial resolution ( $\sim 1^\circ$ ).

<sup>2</sup> [http://heasarc.gsfc.nasa.gov/docs/suzaku/analysis/pin\\_cxb.html](http://heasarc.gsfc.nasa.gov/docs/suzaku/analysis/pin_cxb.html)

<sup>3</sup> [http://www-glast.slac.stanford.edu/software/IS/glast\\_lat\\_performance.htm](http://www-glast.slac.stanford.edu/software/IS/glast_lat_performance.htm)

With Chandra, Townsley et al. (2005) found that the diffuse X-ray emission from Westerlund 2 can be represented by three thermal components ( $kT = 0.1, 0.8,$  and  $3.1$  keV), which is consistent with our 3T model (Table 2). Townsley et al. (2005) indicated that the hottest component can be replaced with a power-law component ( $\Gamma = 2.3$ ). This photon index is also consistent with that in Table 2. Townsley et al. (2005) estimated that the flux of the power-law component is  $1.4 \times 10^{-12}$  ergs cm $^{-2}$  s $^{-1}$  (0.7–10 keV). The difference from our best-fit value ( $f_{\text{NT}} = 5.4 \times 10^{-12}$  ergs cm $^{-2}$  s $^{-1}$ ; see Table 2) could be due to the difference of the regions investigated, and the backgrounds adopted. Townsley et al. (2005) focused on a narrower region ( $\lesssim 5'$  from the center of Westerlund 2), and they took a background in the same Chandra field. Thus, the flux should be regarded as an lower limit. On the other hand, since the power-law component can be replaced by a thermal component, the flux could also be regarded as an upper limit (Figure 5).

With the high-quality of the Suzaku spectrum and the wide region we covered, we think that we have obtained the strictest upper limit of the diffuse non-thermal emission from Westerlund 2 so far.

#### 4.3. Comparison with Theoretical Models of Particle Acceleration

Since Westerlund 2 has more than ten O stars and two Wolf-Rayet (WR) stars (Rauw et al. 2007), the strong winds from them may currently accelerate particles, which may be responsible for the TeV gamma-ray emission from the cluster. Considering the source extension, it is unlikely that a single star produces the gamma-ray emission (Aharonian et al. 2007). Bednarek (2007) and Manolakou et al. (2007) calculated broad band spectra of Westerlund 2; they chose parameters so that the spectra are consistent with previous gamma-ray and X-ray observations. They predicted that synchrotron emission from accelerated electrons could be observed in the X-ray band. Assuming that the distance to Westerlund 2 is 8 kpc and particles are injected uniformly during the lifetime of a WR star, Bednarek (2007) predicted that the X-ray flux would be  $1.3 \times 10^{-11}$  ergs cm $^{-2}$  s $^{-1}$  at  $\sim 1$  keV. Assuming that the distance to the cluster is 2.8 kpc, Manolakou et al. (2007) predicted that the X-ray flux would be  $\sim 2\text{--}3 \times 10^{-11}$  ergs cm $^{-2}$  s $^{-1}$  at  $\sim 1$  keV, depending on the injection time-scale. On the other hand, our new Suzaku results show that the upper limit of the non-thermal emission is  $f_{\text{NT}} < 2.6 \times 10^{-12}$  ergs cm $^{-2}$  s $^{-1}$  (0.7–2 keV), which is much smaller than the above predictions (Figure 5). It would be difficult to adjust the parameters of the theoretical models to match both the new X-ray constraint and the previous gamma-ray observations, because the models must satisfy the relatively large ratio of gamma-ray to X-ray energy flux.

Recently, Fukui et al. (2009) discovered jet and arc-like molecular feature around Westerlund 2. In particular, the latter suggests a past stellar explosion (or past stellar explosions) in the cluster. Based on this observation, we consider particle acceleration associated with the explosion.

The total mass of the molecular gas around Westerlund 2 is  $\sim 2 \times 10^5 M_\odot$  and the size is  $\sim 30$  pc (Furukawa et al. 2009). If the molecular cloud before the explosion of the star had almost the same mass and size, the average proton number density is  $\sim 100 \text{ cm}^{-3}$ . If the star explodes  $\sim 5 \times 10^5$  yrs ago in the molecular cloud with the kinetic energy of  $10^{51}$  erg, the current velocity and radius of the shock wave is  $\sim 16 \text{ km s}^{-1}$  and  $\sim 40$  kpc, respectively (see equation 2 in Yamazaki et al. 2006. The radius can be obtained by the integration of the velocity). The velocity is comparable to the internal velocity of the molecular gas, and the size is comparable to that of the arc ( $\sim 30$  pc) observed around Westerlund 2 (Fukui et al. 2009). Although the shock may still be expanding, it is unlikely that particles are accelerated at the shock at present because of the small velocity. However, particles might be accelerated in the past when the velocity of the shock was large. If adiabatic energy loss did not much affect the particle energy, the accelerated protons should not have lost their energy because of their long cooling time. Thus, the protons accelerated in the past may be producing the TeV gamma-rays through  $pp$ -interactions in the surrounding molecular gas. On the other hand, accelerated electrons should have lost their energy through synchrotron emission. Therefore, the current ratio of gamma-ray to X-ray energy flux should be large, because the electrons are the source of the X-ray flux through synchrotron emission (Yamazaki et al. 2006). This is consistent with the observations of Westerlund 2; the observed ratio of the 1–10 TeV energy flux to the 2–10 keV energy flux is  $R_{\text{TeV/X}} > 2.7$ , which actually indicates that the stellar explosion did not happen recently (Yamazaki et al. 2006). Such stellar explosions in dense clouds could be the sources of unidentified TeV sources and the so-called PAMELA anomaly (Bamba et al. 2009; Ioka & Meszaros 2009; Fujita et al. 2009).

The mass of the star responsible for the explosion could be extremely large, because stars in an open cluster form almost simultaneously and massive stars with  $\sim 80 M_\odot$  still survive in Westerlund 2 (Rauw et al. 2005). In general, such massive stars produce ejecta with a large  $\alpha$ -element to iron abundance ratio (Kobayashi et al. 2006). This trend is consistent with the metal abundances shown in Table 2, although the contribution from stellar winds from surviving stars must be considered for detailed analysis. If the thermal gas in 3T model is uniformly distributed within  $8'$  from the cluster center, the total gas mass is  $890^{+160}_{-290} M_\odot$ . From the metal abundances in Table 2, the masses of Si and S contained in the gas are estimated to be  $\sim 0.1$ – $0.6 M_\odot$  and  $\sim 0.1$ – $0.7 M_\odot$ , respectively. Since a star with a mass of  $\gtrsim 40 M_\odot$  produces  $\sim 0.3 M_\odot$  of Si and  $\sim 0.1 M_\odot$  of S (Kobayashi et al. 2006), explosions of a few massive stars are enough to produce observed Si and S, even if metals that originate from sources other than the stellar explosions are not considered. Since some of the stars with masses of  $\gtrsim 30 M_\odot$  explode as hypernovae (Galama et al. 1998; Iwamoto et al. 1998), the one exploded in Westerlund 2 might be such a hypernova and might trigger a gamma-ray burst. However, because of the large errors for the metal abundances in Table 2 and the lack of the knowledge about the mass of the progenitor star, we cannot firmly determine whether the progenitor star is a supernova

or a hypernova from the metal abundances (Kobayashi et al. 2006).

It is to be noted that pure hadronic models could not account for the GeV gamma-ray radiation detected by EGRET at the position of Westerlund 2 (Hartman et al. 1999; Bednarek 2007). In the near future, Fermi will reveal whether the GeV gamma-ray source is related to the TeV gamma-ray source in Westerlund 2 and by what mechanism the gamma-ray radiation is produced (Figure 5).

## 5. Conclusion

We observed the young open cluster Westerlund 2 with Suzaku X-ray satellite. We found that diffuse X-ray emission extends to  $\sim 8'$  from the cluster center. We analyze the spectrum considering the contamination from point sources using Chandra data. We found that the diffuse emission consists of three thermal components ( $kT \sim 0.1, 0.9,$  and  $4$  keV) or two thermal components ( $kT \sim 0.1$  and  $1.0$  keV) and one non-thermal component ( $\Gamma \sim 2.2$ ). The upper limit of the non-thermal energy flux is smaller than the TeV gamma-ray energy flux observed with H.E.S.S. The abundances of  $\alpha$ -elements are relatively high in comparison with that of iron.

The relatively high X-ray to gamma-ray energy flux ratio suggests that the gamma-ray emission is attributed to protons that were accelerated in the past, because the cooling time of the high-energy protons is much longer than that of high-energy electrons, and the electrons that are responsible for synchrotron X-ray emission may have cooled. Considering the structures in molecular gas surrounding the cluster, protons would have been accelerated at a shock created through a stellar explosion that happened  $\sim 10^5$ – $10^6$  yrs ago. Since extremely massive stars ( $\sim 80 M_\odot$ ) still survive in this cluster, the star responsible for the explosion would also have been very massive. The high abundances of  $\alpha$ -elements compared with iron may support this idea. Thus, the progenitor star could have exploded as a hypernova rather than as a normal supernova.

We wish to thank M. Tsujimoto for providing us the Chandra data. We also thank K. Hamaguchi, and Y. Hyodo for useful discussion. This work was supported in part by a Grant-in-aid from the Ministry of Education, Culture, Sports, Science, and Technology (MEXT) of Japan, No. 20540269 (Y. F.).

## References

- Abdo, A. A., et al. 2007, ApJL, 658, L33
- Aharonian, F., et al. 2002, A&A, 393, L37
- Aharonian, F. A., et al. 2004, Nature, 432, 75
- Aharonian, F., et al. 2007, A&A, 467, 1075
- Anchordoqui, L. A., Beacom, J. F., Goldberg, H., Palomares-Ruiz, S., & Weiler, T. J. 2007, Physical

- Review Letters, 98, 121101
- Ascenso, J., Alves, J., Beletsky, Y., & Lago, M. T. V. T. 2007, *A&A*, 466, 137
- Bamba, A., Yamazaki, R., Kohri, K., Matsumoto, H., Wagner, S., Pühlhofer, G., & Kosack, K. 2009, *ApJ*, 691, 1854
- Bednarek, W. 2003, *MNRAS*, 345, 847
- Bednarek, W. 2007, *MNRAS*, 382, 367
- Belloni, T., & Mereghetti, S. 1994, *A&A*, 286, 935
- Broos, P. S., Townsley, L. K., Getman, K., & Bauer, F. E. 2002, ACIS Extract, An ACIS Point Source Extraction Package (University Park: The Pennsylvania State Univ.) [http://www.astro.psu.edu/xray/docs/TARA/ae\\_users\\_guide.html](http://www.astro.psu.edu/xray/docs/TARA/ae_users_guide.html)
- Dame, T. M. 2007, *ApJL*, 665, L163
- Dickey, J. M., & Lockman, F. J. 1990, *ARA&A*, 28, 215
- Ebisawa, K., et al. 2005, *ApJ*, 635, 214
- Ezoe, Y., Hamaguchi, K., Gruendl, R. A., Chu, Y.-H., Petre, R., & Corcoran, M. F. 2009, *PASJ*, 61, 123
- Fujita, Y., Kohri, K., Yamazaki, R., & Ioka, K. 2009, arXiv:0903.5298
- Fukui, Y., Furukawa, N., Dame, T.M., Dawson, J.R., Yamamoto, H., Rowell, G.P., Aharonian, F., Hofmann, W., de Oña Wilhelmi, E., Minamidani, T., Kawamura, A., Mizuno, N., Onishi, T., Mizuno, A., and Nagataki, S.: 2009, arXiv:0903.5340.
- Furukawa, N., Dawson, J. R., Ohama, A., Kawamura, A., Mizuno, N., Onishi, T., & Fukui, Y. 2009, *ApJL*, 696, L115
- Galama, T. J., et al. 1998, *Nature*, 395, 670
- Getman, K. V., et al. 2005, *ApJS*, 160, 319
- Giovannelli, F., Bednarek, W., & Karakula, S. 1996, *Journal of Physics G Nuclear Physics*, 22, 1223
- Goldwurm, A., Caraveo, P. A., & Bignami, G. F. 1987, *ApJ*, 322, 349
- Hamaguchi, K., et al. 2007, *PASJ*, 59, 151
- Hartman, R. C., et al. 1999, *ApJS*, 123, 79
- Hertz, P., & Grindlay, J. E. 1984, *ApJ*, 278, 137
- Hyodo, Y., Tsujimoto, M., Hamaguchi, K., Koyama, K., Kitamoto, S., Maeda, Y., Tsuboi, Y., & Ezoe, Y. 2008, *PASJ*, 60, 85
- Ioka, K., & Meszaros, P. 2009, arXiv:0901.0744
- Ishisaki, Y., et al. 2007, *PASJ*, 59, 113
- Iwamoto, K., et al. 1998, *Nature*, 395, 672
- Kalberla, P. M. W., Burton, W. B., Hartmann, D., Arnal, E. M., Bajaja, E., Morras, R., Pöppel, W. G. L. 2005, *A&A*, 440, 775
- Koyama, K., et al. 2007, *PASJ*, 59, 23
- Koyama, K., Petre, R., Gotthelf, E. V., Hwang, U., Matsuura, M., Ozaki, M., & Holt, S. S. 1995, *Nature*, 378, 255
- Kobayashi, C., Umeda, H., Nomoto, K., Tominaga, N., & Ohkubo, T. 2006, *ApJ*, 653, 1145
- Kushino, A., Ishisaki, Y., Morita, U., Yamasaki, N. Y., Ishida, M., Ohashi, T., & Ueda, Y. 2002, *PASJ*, 54, 327

- Manolakou, K., Horns, D., & Kirk, J. G. 2007, *A&A*, 474, 689
- Mitsuda, K., et al. 2007, *PASJ*, 59, 1
- Nazé, Y., Rauw, G., & Manfroid, J. 2008, *A&A*, 483, 171
- Piatti, A. E., Bica, E., & Claria, J. J. 1998, *A&AS*, 127, 423
- Rauw, G., et al. 2005, *A&A*, 432, 985
- Rauw, G., Manfroid, J., Gosset, E., Nazé, Y., Sana, H., De Becker, M., Foellmi, C., & Moffat, A. F. J. 2007, *A&A*, 463, 981
- Revnivtsev, M., Sazonov, S., Churazov, E., Forman, W., Vikhlinin, A., & Sunyaev, R. 2009, *Nature*, 458, 1142
- Revnivtsev, M., Sazonov, S., Gilfanov, M., Churazov, E., & Sunyaev, R. 2006, *A&A*, 452, 169
- Snowden, S. L., Egger, R., Finkbeiner, D. P., Freyberg, M. J., & Plucinsky, P. P. 1998, *ApJ*, 493, 715
- Tawa, N., et al. 2008, *PASJ*, 60, 11
- Torres, D. F., Domingo-Santamaría, E., & Romero, G. E. 2004, *ApJL*, 601, L75
- Townsley, L. K., Feigelson, E. D., Montmerle, T., Broos, P. S., Chu, Y.-H., & Garmire, G. P. 2003, *ApJ*, 593, 874
- Townsley, L. K., Feigelson, E. D., Montmerle, T., Broos, P. S., Chu, Y.-H., Garmire, G. P. & Getman K. 2005, in Sjouwerman L. O., Dyer K. K., eds, *Proc. X-ray and Radio Connections*, Santa Fe, [http://www.aoc.nrao.edu/events/xraydio/meetingcont-/3.4\\_townsley.pdf](http://www.aoc.nrao.edu/events/xraydio/meetingcont-/3.4_townsley.pdf)
- Tsujimoto, M., et al. 2007, *ApJ*, 665, 719
- Whiteoak, J. B. Z., & Uchida, K. I. 1997, *A&A*, 317, 563
- Yamazaki, R., Kohri, K., Bamba, A., Yoshida, T., Tsuribe, T., & Takahara, F. 2006, *MNRAS*, 371, 1975